Letter

Dual-Frequency Doppler LiDAR Based on External Optical Feedback Effect in a Laser

Zhuqiu Chen, Yanguang Yu *, Yuxi Ruan, Bairun Nie, Jiangtao Xi, Qinghua Guo and Jun Tong

School of Electrical, Computer and Telecommunications Engineering, University of Wollongong, Northfields Avenue, Wollongong 2522, NSW, Australia; zc606@uowmail.edu.au (Z.C.); yr776@uowmail.edu.au (Y.R.); bn807@uowmail.edu.au (B.N.); jiangtao@uow.edu.au (J.X.); qguo@uow.edu.au (Q.G.); jtong@uow.edu.au (J.T.)
* Correspondence: yanguang@uow.edu.au; Tel.: +61-2-4221-8187

Abstract: A novel Dual-frequency Doppler LiDAR (DFDL) is presented where the dual-frequency light source is generated by using external optical feedback (EOF) effect in a laser diode (LD). By operating a LD at period-one (P1) state and choosing suitable LD related parameters, a dual-frequency light source can be achieved. Such a dual-frequency source has advantages of the minimum part-count scheme, low cost in implementation, and ease in optical alignment. Theory and system design are presented for the proposed DFDL for velocity measurement with high measurement resolution. The proposed design has a potential contribution to the Light Detection And Ranging (LiDAR) in practical engineering applications.

Keywords: doppler LiDAR; dual-frequency laser; optical feedback; velocity measurement; laser dynamics

1. Introduction

Light Detection And Ranging (LiDAR) is a method for measuring distances (ranging) by illuminating the target with laser light and measuring the reflection with a sensor [1]. LiDAR systems have been widely investigated and used since the 1970s. Its advantages such as good directionality, high spatial resolution, and noninvasive in velocity detection have enabled LiDAR to be extensively employed in numerous applications [2]. In remote sensing, LiDARs are coupled with visual sensors to build highly robust scan-matching approaches aiming to achieve simultaneous localization and mapping (SLAM). LiDARs are able to provide high resolution when assessing building damages caused by earthquakes. Wind LiDARs are used in measurements of the atmospheric turbulence. In modeling and imaging, LiDAR applications include scene reconstruction and terrain modeling with high quality utilizing cameras-LiDARs fusion in planetary and terrestrial robotics [3–6]. In the early stage of LiDAR systems, the backscattered single frequency laser light reflected by the moving target and would utilize the Doppler effect. The velocity information can be extracted from the Doppler shift frequency through signal processing technology [7–9]. The single frequency Doppler LiDAR systems have the ability to measure wind velocities with a deviation over ranges of up to 0.39 m/s [10], to achieve the atmospheric measurement over a 51-day continuous and unattended field deployment with a range of 7.5 km for observing the boundary layer [11], and detect air turbulence in clear air at a range of 9.3 km at cruising altitudes [12]. However, they are highly sensitive to external disturbances. For example, the spectral bandwidth of the Doppler-shifted line could be broadened by speckle noise and optical noise caused by the roughness of the target and the coherence properties of a laser. Consequently, the velocity measurement resolution will be degraded. To overcome these disadvantages, an alternative solution

known as Dual-frequency Doppler LiDAR (DFDL) has emerged. This approach utilizes a microwave beat frequency which contains two optical frequency components [13–16]. The velocity of a moving target can be measured by identifying the difference of doppler frequency shifts of two frequency components. Currently, the generation of dual-frequency can be achieved in a number of ways, e.g., utilizing dual-frequency laser that emits dual-frequency laser beam by inserting two quarter-wave plates inside the laser cavity; Combining two single-frequency laser beams to create a dual-frequency laser beam; Injecting two single-frequency beams from two master lasers into one slave laser; Using one pair of master-slave lasers, where the slave laser is operating in period-one oscillation state to emit dual-frequency [15,17–20]. However, these methods require two or more laser diodes (LDs) for generating dual-frequency. The method in [19] requires only one LD but an expensive frequency shifter (acousto-optic modulator) is needed. These requirements lead to a complicated and expensive system.

In this paper, we proposed a new method to generate a dual-frequency source by using laser dynamics. Laser diodes (LD) with external optical feedback (EOF) are known to demonstrate complex dynamics, which may give rise to negative effects on the LD performance, e.g., degrading the modulation response characteristics, enhancing laser intensity noise, etc [21]. Meanwhile, such EOF effect in a LD also enables many applications, e.g., a class of laser interferometry, termed optical feedback interferometry, or self-mixing interferometry (SMI). As a promising non-contact sensing technology, EOF has attracted intensive research in recent decades due to the merits of the minimum part-count scheme, low cost in implementation, and ease in optical alignment [22–26]. With the increase of the optical feedback, a LD will leave the steady state and enter other dynamic states such as period-one (P1) oscillation, multi-periodic oscillation, and chaos, and rich dynamics can then be observed [27]. In recent years, LD dynamics have been investigated and found their various potential applications in high-resolution sensing, photonic microwave generation, balance detection, chaotic radar, etc. [28–33]. In this paper, a novel DFDL system is proposed. The dual-frequency is generated by using a LD with EOF operating at P1 state. The related theory design and analysis are presented. The results show that the proposed DFDL system can reach up to 4.8 µm/s velocity measurement resolution with 31.21 GHz microwave beat frequency.

2. Generation of Dual-Frequency Laser

Laser dynamics induced by EOF is studied by using the set up shown in Figure 1. It consists of a LD and an external target. The length between the LD front facet and the external target is defined as the external cavity length denoted by *L*. The laser intensity is captured by an external photodiode (PD).
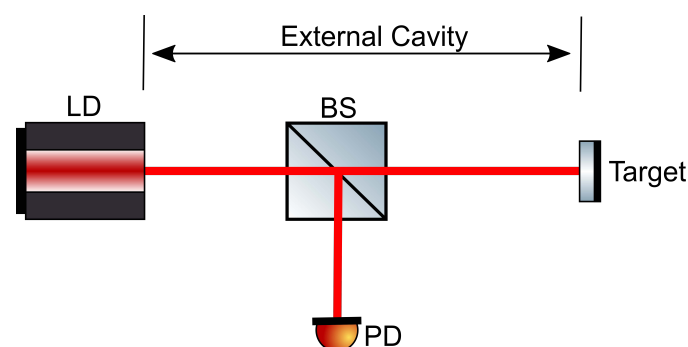

Figure 1. Schematic diagram of a laser diode (LD) with the external optical feedback (EOF) system.

The dynamics of an EOF system can be described by the well-known Lang and Kobayashi (L-K) equations, as shown in Equations (1)–(3) [34]. In which $E(t)$ is the amplitude of the electric field, $\phi(t)$ is the electric field phase, and $N(t)$ is the carrier density.

$$\frac{dE(t)}{dt} = \frac{1}{2}\left\{G[N(t), E(t)] - \frac{1}{\tau_p}\right\}E(t) + \frac{\kappa}{\tau_{in}} \cdot E(t-\tau) \cdot \cos[\omega_0\tau + \phi(t) - \phi(t-\tau)] \tag{1}$$

$$\frac{d\phi(t)}{dt} = \frac{1}{2}\alpha\left\{G[N(t), E(t)] - \frac{1}{\tau_p}\right\} - \frac{\kappa}{\tau_{in}} \cdot \frac{E(t-\tau)}{E(t)} \cdot \sin[\omega_0\tau + \phi(t) - \phi(t-\tau)] \quad (2)$$

$$\frac{dN(t)}{dt} = \frac{J}{eV} - \frac{N(t)}{\tau_s} - G[N(t), E(t)]E^2(t) \quad (3)$$

where $G[N(t), E(t)] = G_N[N(t) - N_0][1 - \varepsilon\Gamma E^2(t)]$ is the modal gain per unit time. Physical meanings and values of parameters used in Equations (1)–(3) can be found in Table 1.

Table 1. Physical meanings of symbols in Lang and Kobayashi (L-K) equations [33].

	Symbol	Physical Meaning	Value
LD Internal Parameters	G_N	Model gain coefficient	$8.1 \times 10^{-13}\,\mathrm{m^3 s^{-1}}$
	N_0	Carrier density at transparency	$1.1 \times 10^{24}\,\mathrm{m^{-3}}$
	ε	Nonlinear gain compression coefficient	$2.5 \times 10^{-23}\,\mathrm{m^3}$
	Γ	Confinement factor	0.3
	τ_p	Photon lifetime	$2.0 \times 10^{-12}\,\mathrm{s}$
	τ_s	Carrier lifetime	$2.0 \times 10^{-9}\,\mathrm{s}$
	τ_{in}	Internal cavity round-trip time	$8.0 \times 10^{-12}\,\mathrm{s}$
	e	Elementary charge	$1.6 \times 10^{-19}\,\mathrm{C}$
	V	Volume of the active region	$1 \times 10^{-16}\,\mathrm{m^3}$
	ω_0	Unperturbed optical angular frequency of a laser diode, $\omega_0 = 2\pi c/\lambda_0$, where c is the speed of light, λ_0 is the wavelength of the LD	
	α	Line-width enhancement factor	
LD Controllable Parameters	J	Injection current	
	κ	Feedback strength	
	L	External cavity length	
	τ	External cavity round trip time, $\tau = 2L/c$	

The parameters shown in Table 1 can be classified as LD internal parameters that are fixed values for a given LD, and controllable parameters associated with the external cavity and LD states. The laser intensity $E^2(t)$ can be obtained through numerical solving the L-K equations. The LD dynamics states can be identified by observing the waveform of $E^2(t)$.

Through changing one or more controllable parameters, a LD may experience different dynamic states, including steady state, P1 oscillation state, period-doubling oscillation state, and chaos. The routing from steady state to chaos when a specific parameter change is called bifurcation. To generate a bifurcation diagram, the local maximum (or minimum) of the waveform of $E^2(t)$ denoted by $E_{\max}^2(t)$ are sampled for a set parameters given for a LD and its external cavity. As an example, Figure 2 presents a bifurcation diagram with parameters: $\alpha = 3$, $L = 11$ cm and $J = 1.3J_{th}$ (J_{th} is the LD current threshold), other parameter values refer to Table 1. As we are interested in how the EOF strength κ influences the LD states. Hence, we vary κ from 0 to 0.025 with a step size of 0.0001. At each feedback strength κ, we obtained the corresponding LD state and present it on the bifurcation diagram in a 2-D plane ($E_{\max}^2(t)$, κ) on Figure 2, different states are indicated with corresponding κ ranges.

It can be seen from Figure 2, the steady state corresponds to the range of κ with $0 < \kappa < 0.0069$. With the further increase of κ, undamped relaxation oscillation will occur after the Hopf bifurcation point, which causes the system to enter the P1 oscillation state region with $0.0069 < \kappa < 0.0124$, and routes to period-2 (P2) state with $0.0124 < \kappa < 0.0175$, period-4 (P4) state with $0.0175 < \kappa < 0.0207$. Eventually, due to the large κ, the system collapsed and presents chaos state when $\kappa > 0.0207$. Generally, P2 and P4 states can also be collectively referred to as period-doubling.

Next, let us make an investigation on how to generate a dual-frequency laser signal at P1 state. Both feedback strength κ and external cavity length L are varying and are treated as control parameters for LD state. The cavity length L starts from 14 cm to 18 cm with a step of 0.1 cm. For each L, κ increase

from 0 to 0.025 with a step size of 0.0001. By observing the waveform of $E^2(t)$, the corresponding LD states are recorded and indicated on the (κ, L) plane shown in Figure 3.
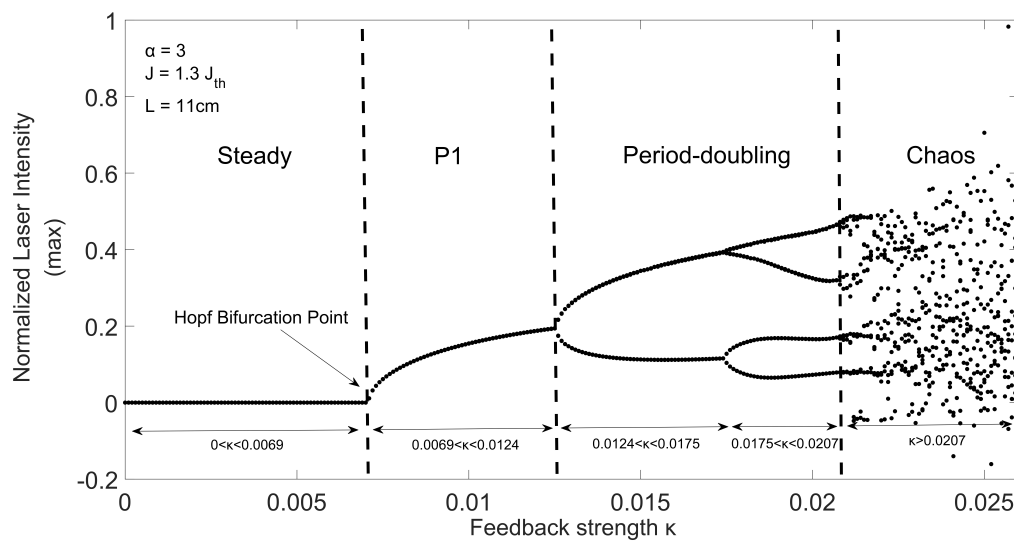
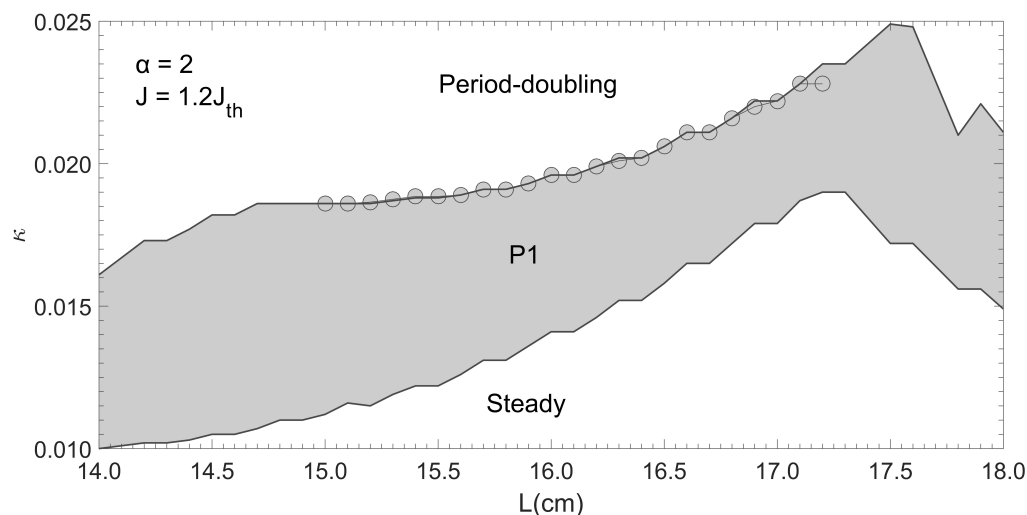**Figure 2.** Bifurcation diagram for a LD with EOF system.

Figure 3. State diagram under the parameter space (κ, L).

The circles shown in Figure 3 indicate the corresponded (κ, L) values with which the LD is able to generate a dual-frequency laser signal. We found the region that can generate dual-frequency to be only within $L = 15.0$ cm to $L = 17.2$ cm and are on the boundary between the P1 region and the period-doubling region. The dual-frequency spectrum will disappear once the external cavity length is beyond the range. The wavelength difference of the two frequency is denoted as $\Delta\lambda = |\lambda_2 - \lambda_1|$, where λ_1 and λ_2 are two corresponding wavelengths of two frequency components f_1 and f_2. Its corresponding frequency is known as beat frequency $f_{beat} = |f_2 - f_1| = |c/\lambda_2 - c/\lambda_1|$. Figure 4 shows eight examples of optical spectrum for dual-frequency laser signals generated for certain (κ, L) parameter pairs. Figure 4a shows the generated two wavelengths are $\lambda_1 = 1550.00$ nm and $\lambda_2 = 1559.13$ nm when $L = 15.0$ cm, which cause a $\Delta\lambda = 9.13$ nm. This results a beat frequency $f_{beat} = 1133.40$ GHz. From Figure 4b–h, we further increase L from 15.1 cm to 17.2 cm, the corresponding wavelength difference $\Delta\lambda$ decrease from 8.46 nm to 0.24 nm.
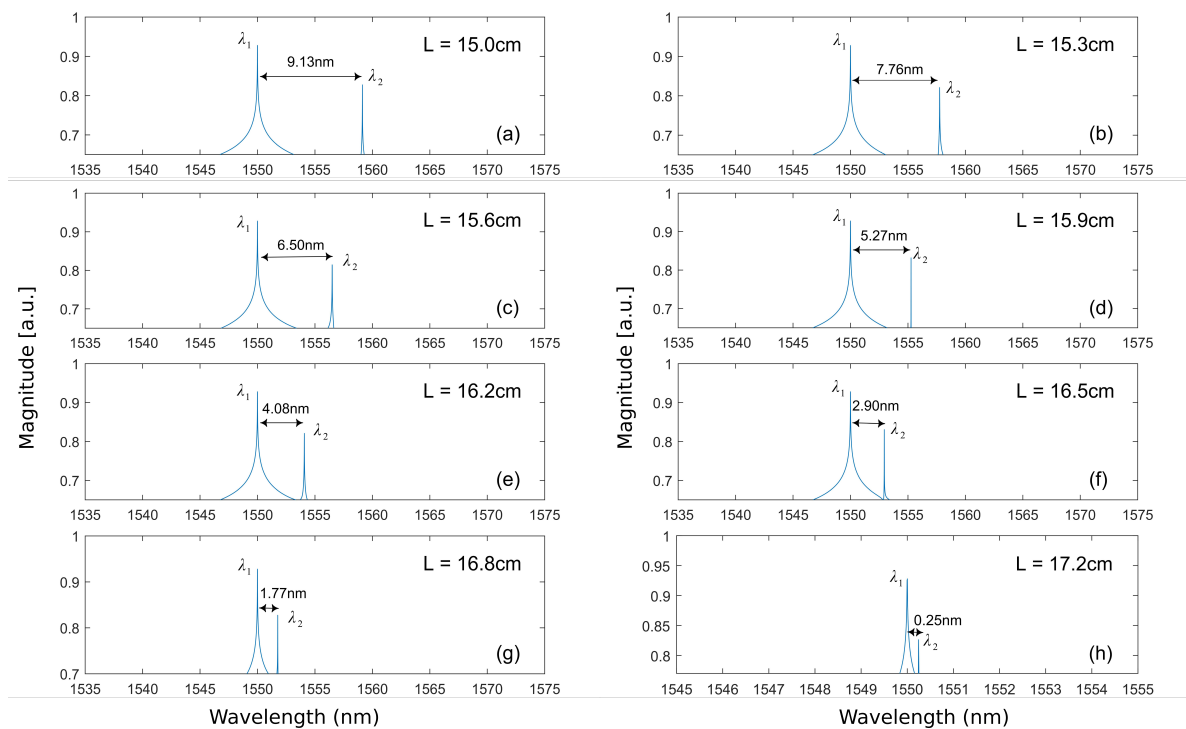
Figure 4. Optical spectrum of the dual-frequency laser signals. (**a**–**h**) with different external cavity length.

We also established the relationship between the f_{beat} and L shown in Figure 5. It shows the f_{beat} changes from 1050.40 GHz to 31.21 GHz with increasing L from 15.1 cm to 17.2 cm. These results show that a tunable microwave frequency can be generated by varying the external length L, which provides flexibility for generating a desired dual-frequency laser signal for different application needs. Besides, results also indicate that it is not a perfect linear decline process. After a period of decline, two consecutives f_{beat} values will be the same. This shows that when a specific f_{beat} is generated in this way, it is robust to adjust the length of the external length L when J and α are fixed.
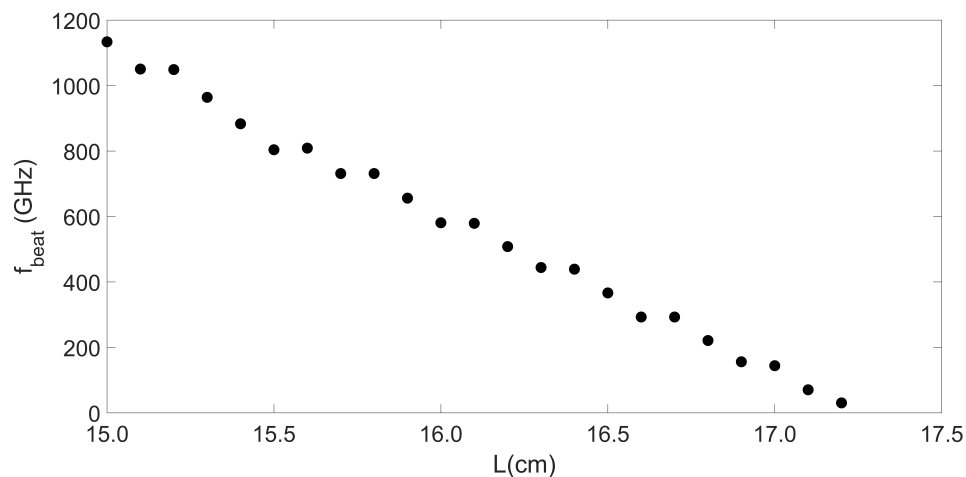

Figure 5. Relationship between f_{beat} and L.

3. Setup and Principle of DFDL System

In Section 2, we have demonstrated that an EOF system operating in P1 state can generate a dual-frequency signal. In this section, we utilized this feature and use it as the dual-frequency light source in the DFDL system. The schematic layout of the DFDL system is depicted in Figure 6. The boxed area is an EOF system that plays a role as the dual-frequency light source, it consists of a LD, a mirror,

and a variable attenuator (VA). By varying the VA to adjust the optical feedback strength, thus, the LD can operate in P1 state to emit dual-frequency light.
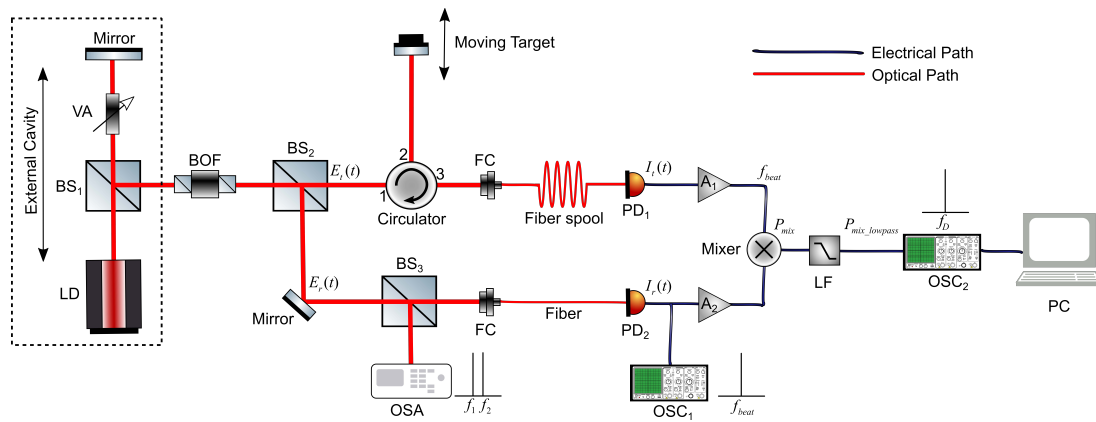

Figure 6. Experimental setup of Dual-frequency Doppler LiDAR (DFDL) system. LD, single-mode laser diode; MFS, microwave frequency synthesizer; BS, beam splitter; VA, variable attenuator; BOF, bandpass optical filter; FC, fiber coupler; Circulator; Fiber and Fiber spool; PD$_1$ and PD$_2$, high-speed photodiodes; A$_1$ and A$_2$, microwave amplifiers; Mixer, microwave mixer; OSC$_1$ and OSC$_2$, digital oscilloscopes; OSA, optical spectrum analyzer; LF, lowpass filter; PC, computer.

A fraction of the laser beam from the LD is divided by beam splitter BS$_1$, then directed to a bandpass optical filter (BOF), this is to reduce the sidebands and noise in the dual-frequency light. Then the light is split into two beams again by BS$_2$, one beam named target measurement beam with the electric field $E_t(t)$ is sent to the port 1 of a circulator and comes out from port 2, then it is reflected by a target moving with a constant speed v. The moving target will introduce the Doppler effect and results in a frequency shift of the generated beat frequency signal f_{beat} denoted as $f_D = \left| f_{D2} - f_{D1} \right|$, where f_{D1} and f_{D2} are Doppler shift frequency of f_1 and f_2, respectively. f_D is also called Doppler shift frequency difference. Then, the light with the electric field $E_t(t)$ comes out from port 3 and is coupled into a long length fiber spool (in tens of km). PD$_1$ transfers electric field to photocurrent denoted as $I_t(t)$. Another beam from BS$_2$ named as reference beam with the electric field $E_r(t)$ is then split again by BS$_3$ and directed to an optical spectrum analyzer (OSA) and PD$_2$ respectively. The OSA is used to visualize the dual-frequency laser spectrum (with components f_1 and f_2). The output photocurrent of PD$_2$ with the frequency f_{beat} is denoted as $I_r(t)$ and its electrical spectrum can be recorded by the oscilloscope OSC$_1$ to get f_{beat}. Both photocurrents $I_t(t)$ and $I_r(t)$ from PD$_1$ and PD$_2$ are boosted by microwave amplifiers denoted by A$_1$ and A$_2$ with gain factor M_1 and M_2, and then mixed inside a microwave mixer. The output of the mixer is sent to the OSC$_2$ to acquire the Doppler signal and recorded on a PC, from which f_D can be measured.

The dual-frequency light containing two optical frequencies components (f_1 and f_2) are with light magnitude as E_1 and E_2, respectively. For the reference beam, the electric field of the dual-frequency signal can be expressed as,

$$E_r(t) = E_1 e^{i[\phi_1(t) - 2\pi f_1 t]} + E_2 e^{i[\phi_2(t) - 2\pi f_2 t]} \tag{4}$$

where $\phi_1(t)$ and $\phi_2(t)$ are the two optical phases relating to the two frequency components f_1 and f_2, respectively. Then, for the target measurement beam, the signal received at the PD$_1$ can be expressed as below, a delay τ (round trip) is caused due to the moving target. This is written as,

$$E_t(t) = E_1 e^{i[\phi_1(t-\tau) - 2\pi f_1(t-\tau)]} + E_2 e^{i[\phi_2(t-\tau) - 2\pi f_2(t-\tau)]} \tag{5}$$

where $\tau = 2p/c$ is the round-trip delay time, $p = d + vt$ is the target position, d is the initial distance of the target, v is the speed of the moving target. The detected current signals from PD_1 and PD_2, respectively, are expressed as,

$$I_t(t) = 2M_1 E_1 E_2 \cos[2\pi f_{beat} t - 4p\pi f_{beat}/c - \Delta\phi(t - \tau)] \tag{6}$$

$$I_r(t) = 2M_2 E_1 E_2 \cos[2\pi f_{beat} t - \Delta\phi(t)] \tag{7}$$

where M_1 and M_2 are the amplifier gain for the target beam applied by microwave amplifier A_1 and A_2, respectively, $\Delta\phi(t) = \phi_2(t) - \phi_1(t)$. After passing A_1 and A_2, two current signals are sent to a microwave mixer and outputting a signal P_{mix}, which is proportional to the product of $I_r(t)$ and $I_t(t)$. According to Equations (6) and (7), the product of $I_r(t)$ and $I_t(t)$ is shown below,

$$\begin{aligned} P_{mix} = {} & I_r(t) * I_t(t) \\ = {} & 2M_1 M_2 E_1^2 E_2^2 \cos(2\pi f_D t + 4\pi d f_{beat}/c - \Phi) + \\ & 2M_1 M_2 E_1^2 E_2^2 \cos[2\pi(2f_{beat} - f_D)t - 4\pi d f_{beat}/c - \Delta\phi(t) - \Delta\phi(t - \tau)] \end{aligned} \tag{8}$$

where $\Phi = \Delta\phi(t) - \Delta\phi(t - \tau)$. It can be seen, the first term in Equation (8) is with low frequency (with frequency f_D dominated) and the second term is with very high frequency dominated by $(2f_{beat} - f_D)$ in GHz. If we make use of the low-frequency component contained in the signal P_{mix}, after a lowpass filter processing, we have,

$$P_{mix\_lowpass} = 2M_1 M_2 E_1^2 E_2^2 \cos(2\pi f_D t + 4\pi d f_{beat}/c - \Phi) \tag{9}$$

f_D can be obtained by taking the power spectral density (PSD) on the signal $P_{mix\_lowpass}$. Then the velocity of the moving target can be calculated by,

$$v = c f_D / 2 f_{beat} \tag{10}$$

Regarding f_{beat}, it is determined by the dual-frequency source system demonstrated in Section 2. As an example, with the parameters setting for the LD given in Figure 4h, $\alpha = 2$, $J = 1.2J_{th}$, $L = 17.2$ cm, and $\kappa = 0.0228$, the system is able to generate a dual-frequency light shown in Figure 7. Figure 7a is the laser intensity ($E^2(t)$) waveform. Figure 7b shows an enlargement region in Figure 7a for the time duration from 1 μs to 1.02 μs. Figure 7c shows the optical spectrum containing two wavelengths with $\lambda_1 = 1550.00$ nm, $\lambda_2 = 1550.25$ nm. The wavelength difference is $\Delta\lambda = 0.25$ nm. Thus, the beat frequency f_{beat} is 31.21 GHz. The velocity measurement resolution corresponds to the measurement resolution of f_D. For instance, if we use Tektronix RSA7100B spectrum analyzer to measure f_D, the frequency measurement resolution will be 1×10^{-3} Hz. This will work out a corresponding velocity resolution as 4.8 μm/s. In Table 2, we show a comparison of our proposed DFDL to some of other dual-frequency methods, it is evident that our proposed DFDL provided a great improvement on velocity measurement resolution.
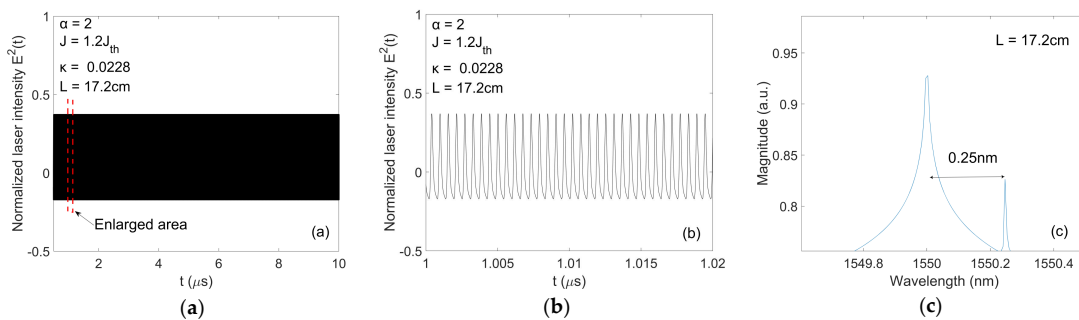

Figure 7. (**a**) LD operates at P1 state; (**b**) Enlargement of boxed area in (**a**); (**c**) Optical spectrum of laser light with two frequency components.

Table 2. Comparison between our DFDL system and existing dual-frequency methods.

	This Work	[35]	[14]	[36]	[37]	[16]
Velocity measurement resolution	4.8 μm/s	26 μm/s	310 μm/s	327.9 μm/s	7.5×10^4 μm/s	1.2×10^6 μm/s

4. Conclusions

With the change of one or more controllable system parameters in EOF system, such as injection current J, feedback strength κ, external cavity L, the LD will undergo from steady state, P1 state, period-doubling state, and chaos state. At steady state, there is only one optical frequency component emitted by a LD. However, as the laser experiences the Hopf bifurcation and enters the P1 state, a second dominant optical frequency component will appear. This is how the dual-frequency is generated in a LD with EOF. Our analysis shows that the dual-frequency varies with the external cavity length. This provides the flexibility for users to generate the desired beat frequency signals to suit practical needs. By using the proposed dual-frequency source, a novel Doppler LiDAR is presented for velocity measurement. The proposed design combines the merits of both the EOF system and DFDL, which have the advantages of low structural complexity, low power consumption, low cost, and light weight. Therefore, it has the potential to provide LiDAR measurement with high sensing resolution and a compact configuration for several practice usage, like in airborne and space-borne applications for velocity measurement. However, the beat frequency f_{beat} generated using the system presented in this paper contains some noise caused by sidebands around the dual frequency components. To improve the measurement performance of the proposed system, some methods need to be explored to achieve narrower line width.

References

1. Dong, P.; Chen, Q. *LiDAR Remote Sensing and Applications*; CRC Press: Boca Raton, FL, USA, 2017.
2. Quackenbush, L.J.; Im, I.; Zuo, Y. Road extraction: A review of LiDAR-focused studies. *Remote Sens. Nat. Resour.* **2013**, *9*, 155–169.
3. Dong, L.; Shan, J. A comprehensive review of earthquake-induced building damage detection with remote sensing techniques. *ISPRS J. Photogramm. Remote Sens.* **2013**, *84*, 85–99. [CrossRef]
4. Sathe, A.; Mann, J. A review of turbulence measurements using ground-based wind lidars. *Atmos. Meas. Tech.* **2013**, *6*, 3147–3167. [CrossRef]
5. Park, K.; Kim, S.; Sohn, K. High-precision depth estimation using uncalibrated LiDAR and stereo fusion. *IEEE Trans. Intell. Transp. Syst.* **2019**, *21*, 321–335. [CrossRef]
6. Debeunne, C.; Vivet, D. A Review of Visual-LiDAR Fusion based Simultaneous Localization and Mapping. *Sensors* **2020**, *20*, 2068. [CrossRef]
7. Chanin, M.; Garnier, A.; Hauchecorne, A.; Porteneuve, J. A Doppler lidar for measuring winds in the middle atmosphere. *Geophys. Res. Lett.* **1989**, *16*, 1273–1276. [CrossRef]
8. Gentry, B.M.; Chen, H.; Li, S.X. Wind measurements with 355-nm molecular Doppler lidar. *Opt. Lett.* **2000**, *25*, 1231–1233. [CrossRef]
9. Frehlich, R.; Cornman, L. Estimating spatial velocity statistics with coherent Doppler lidar. *J. Atmos. Ocean. Technol.* **2002**, *19*, 355–366. [CrossRef]
10. Afanasiev, A.; Banakh, V.; Gordeev, E.; Marakasov, D.; Sukharev, A.; Falits, A. Verification of a passive correlation optical crosswind velocity meter in experiments with a Doppler wind lidar. *Atmos. Ocean. Opt.* **2017**, *30*, 574–580. [CrossRef]

11. Pearson, G.; Davies, F.; Collier, C. An analysis of the performance of the UFAM pulsed Doppler lidar for observing the boundary layer. *J. Atmos. Ocean. Technol.* **2009**, *26*, 240–250. [CrossRef]

12. Eberhard, W.L.; Cupp, R.E.; Healy, K.R. Doppler lidar measurement of profiles of turbulence and momentum flux. *J. Atmos. Ocean. Technol.* **1989**, *6*, 809–819. [CrossRef]

13. Diaz, R.; Chan, S.-C.; Liu, J.-M. Lidar detection using a dual-frequency source. *Opt. Lett.* **2006**, *31*, 3600–3602. [CrossRef] [PubMed]

14. Cheng, C.-H.; Lee, C.-W.; Lin, T.-W.; Lin, F.-Y. Dual-frequency laser Doppler velocimeter for speckle noise reduction and coherence enhancement. *Opt. Express* **2012**, *20*, 20255–20265. [CrossRef] [PubMed]

15. Cheng, C.-H.; Lin, L.-C.; Lin, F.-Y. Self-mixing dual-frequency laser Doppler velocimeter. *Opt. Express* **2014**, *22*, 3600–3610. [CrossRef]

16. Vercesi, V.; Onori, D.; Laghezza, F.; Scotti, F.; Bogoni, A.; Scaffardi, M. Frequency-agile dual-frequency lidar for integrated coherent radar-lidar architectures. *Opt. Lett.* **2015**, *40*, 1358–1361. [CrossRef]

17. Thévenin, J.; Vallet, M.; Brunel, M.; Gilles, H.; Girard, S. Beat-note locking in dual-polarization lasers submitted to frequency-shifted optical feedback. *J. Opt. Soc. Am. B* **2011**, *28*, 1104–1110. [CrossRef]

18. Juan, Y.-S.; Lin, F.-Y. Photonic generation of broadly tunable microwave signals utilizing a dual-beam optically injected semiconductor laser. *IEEE Photonics J.* **2011**, *3*, 644–650. [CrossRef]

19. Kang, Y.; Cheng, L.; Yang, S.; Zhao, C.; Zhang, H.; He, T. 50 W low noise dual-frequency laser fiber power amplifier. *Opt. Express* **2016**, *24*, 9202–9208. [CrossRef]

20. Chen, J.; Zhu, H.; Xia, W.; Guo, D.; Hao, H.; Wang, M. Self-mixing birefringent dual-frequency laser Doppler velocimeter. *Opt. Express* **2017**, *25*, 560–572. [CrossRef]

21. Soriano, M.C.; García-Ojalvo, J.; Mirasso, C.R.; Fischer, I. Complex photonics: Dynamics and applications of delay-coupled semiconductors lasers. *Rev. Mod. Phys.* **2013**, *85*, 421–470. [CrossRef]

22. Donati, S. Developing self-mixing interferometry for instrumentation and measurements. *Laser Photonics Rev.* **2012**, *6*, 393–417. [CrossRef]

23. Li, K.; Cavedo, F.; Pesatori, A.; Zhao, C.; Norgia, M. Balanced detection for self-mixing interferometry. *Opt. Lett.* **2017**, *42*, 283–285. [CrossRef]

24. Shi, L.; Guo, D.; Cui, Y.; Hao, H.; Xia, W.; Wang, Y.; Ni, X.; Wang, M. Design of a multiple self-mixing interferometer for a fiber ring laser. *Opt. Lett.* **2018**, *43*, 4124–4127. [CrossRef] [PubMed]

25. Ruan, Y.; Liu, B.; Yu, Y.; Xi, J.; Guo, Q.; Tong, J. High sensitive sensing by a laser diode with dual optical feedback operating at period-one oscillation. *Appl. Phys. Lett.* **2019**, *115*, 011102. [CrossRef]

26. Amin, S.; Zabit, U.; Bernal, O.D.; Hussain, T. High Resolution Laser Self-Mixing Displacement Sensor under Large Variation in Optical Feedback and Speckle. *IEEE J.* **2020**, *20*, 9140–9147.

27. Uchida, A. *Optical Communication with Chaotic Lasers: Applications of Nonlinear Dynamics and Synchronization*; John Wiley & Sons: Hoboken, NJ, USA, 2012.

28. Zhang, B.; Zhu, D.; Zhou, P.; Xie, C.; Pan, S. Tunable triangular frequency modulated microwave waveform generation with improved linearity using an optically injected semiconductor laser. *Appl. Opt.* **2019**, *58*, 5479–5485. [CrossRef]

29. Zhou, P.; Li, N.; Pan, S. Photonic microwave harmonic down-converter based on stabilized period-one nonlinear dynamics of semiconductor lasers. *Opt. Lett.* **2019**, *44*, 4869–4872. [CrossRef]

30. Zhao, A.; Jiang, N.; Liu, S.; Xue, C.; Qiu, K. Wideband time delay signature-suppressed chaos generation using self-phase-modulated feedback semiconductor laser cascaded with dispersive component. *J. Lightwave Technol.* **2019**, *37*, 5132–5139. [CrossRef]

31. Liu, B.; Ruan, Y.; Yu, Y.; Guo, Q.; Xi, J.; Tong, J. Modeling for optical feedback laser diode operating in period-one oscillation and its application. *Opt. Express* **2019**, *27*, 4090–4104. [CrossRef]

32. Tseng, C.-H.; Hwang, S.-K. Broadband chaotic microwave generation through destabilization of period-one nonlinear dynamics in semiconductor lasers for radar applications. *Opt. Lett.* **2020**, *45*, 3777–3780. [CrossRef]

33. Nie, B.; Ruan, Y.; Yu, Y.; Guo, Q.; Xi, J.; Tong, J. Period-one Microwave Photonic Sensing by a Laser Diode with Optical Feedback. *J. Lightwave Technol.* **2020**, *38*, 5423–5429. [CrossRef]

34. Lang, R.; Kobayashi, K. External optical feedback effects on semiconductor injection laser properties. *IEEE J. Quantum Electron.* **1980**, *16*, 347–355. [CrossRef]

35. Diaz, R.; Chan, S.-C.; Liu, J.-M. Dual-frequency multifunction lidar. In *Free-Space Laser Communication Technologies XIX and Atmospheric Propagation of Electromagnetic Waves*; International Society for Optics and Photonics: Bellingham, WA, USA, 2007; p. 64570.

36. Chen, G.; Lu, D.; Guo, L.; Zhao, W.; Wang, H.; Zhao, L. Dual-frequency Laser Doppler Velocimeter based on Integrated Dual-mode Amplified Feedback Laser. In Proceedings of the Asia Communications and Photonics Conference, Hangzhou, China, 26–29 October 2018; pp. 1–3.

37. Onori, D.; Scotti, F.; Laghezza, F.; Scaffardi, M.; Bogoni, A. Coherent laser radar with dual-frequency Doppler estimation and interferometric range detection. In Proceedings of the IEEE Radar Conference, Philadelphia, PA, USA, 2–6 May 2016; pp. 1–5.